Compatibility of Deformation in Two-Phase Ti-Al Alloys: Dependence on Microstructure and Orientation Relationships

J. LUSTER and M.A. MORRIS

A two-phase alloy of composition Ti-47.5Al-2.5Cr has been studied under two heat-treated conditions in order to obtain different microstructures. These consisted of lamellar and equiaxed distributions of γ grains in which the α_2 phase was distributed as long lamellae or smaller globules, respectively. The specific rotation relationships between γ/γ and γ/α_2 grains have been measured, and these have been used to understand their effect on the compatibility of deformation across adjacent grains. For this, detailed analysis of active slip systems has been carried out by transmission electron microscopy (TEM) observations of deformed samples. A theoretical calculation of a geometric compatibility factor characterizing the best slip transfer across adjacent grains has been used in such a way that it has been possible to deduce the role played by the type of orientation relationship between grains in producing active deformation systems that allow the maximum compatibility of deformation.

I. INTRODUCTION

DURING the past years, significant advances have been made in improving the ductility of two-phase alloys consisting of γ-TiAl and α_2-Ti_3Al.[1] Previous studies have shown that the primary deformation mechanisms in two-phase TiAl alloys are slip of $1/2\langle 110]$ ordinary dislocations and $1/6\langle 112]\ \{111\}$ deformation twinning.[2,3] Fewer $\langle 101]$ and $1/2\langle 112]$ superdislocations are observed in two-phase alloys in comparison with the single-phase counterparts.[4,5] This change in deformation mechanisms has been attributed to an oxygen-gettering effect of the α_2 phase that has been proposed as responsible for the improved ductility of the alloys.[2]

One prevalent feature of these two-phase alloys is the existence of specific orientation relationships between the phases present. In the lamellar microstructure, the alternating γ and α_2 lamellae are oriented such that the following relationships have been confirmed to exist:[5,6]

$$[\bar{2}110]_{\alpha_2}//\langle 011\rangle_\gamma \text{ and } (0001)_{\alpha_2}//\{111\}_\gamma$$

As a consequence of these relationships and due to the phase transformation sequences that occur during the thermomechanical treatments, adjacent lamellae of the γ phase also exhibit a well-defined orientation relationship that can be described by a multiple of 60 deg rotation about a $\langle 111\rangle$ pole.[7] From the six possible orientations, three different types of orientation relationships between adjacent γ grains can be described as a 180 deg true-twin relationship, a 60 deg pseudotwin relationship, and a 120 deg rotation relationship that retains the ABCABC stacking sequence. This 120 deg rotation can be equally well described as a 90 deg rotation about a $\langle 010\rangle$ pole. While a few studies have been carried out to show that the specific orientation relationship between grains makes possible the transmission of slip between adjacent grains,[3,8–10] no systematic studies have been performed in this area. Since the transmission of slip across grain boundaries is expected to play a dominant role in the deformation behavior of the alloys, it appears relevant to relate the latter to the rotation relationships between adjacent grains for different types of microstructure.

In an effort to provide more fundamental understanding regarding the influence of microstructure on the deformation mechanisms of two-phase alloys, a detailed analysis of the active slip systems produced by room-temperature compression has been carried out from both lamellar and equiaxed microstructures using transmission electron microscopy (TEM). The influence that the load orientation with respect to each given grain and that of the orientation relationships between adjacent grains have on the slip systems activated have been systematically compared using a geometric compatibility factor as defined in this section.

The concept of the compatibility factor has been used extensively in the past in order to predict the transfer of slip between adjacent grains in such a way as to maintain coherency at grain boundaries as homogeneous deformation of polycrystalline materials occurred.[12–16] The compatibility between active slip systems in adjacent grains can be defined by a *geometric compatibility factor* that indicates the alignment or similarity of the slip systems. This factor, designated as m', can be calculated from the knowledge of two angles: the angle, κ, between the slip directions in grains I and II and the angle, ϕ, between the normal to the slip planes. A schematic representation of slip systems in adjacent grains is given in Figure 1, where these two angles are clearly shown. The geometric compatibility factor, m', is thus calculated as $m' = \cos\phi \cdot \cos\kappa$.

Using this definition, the geometric compatibility factor between the slip systems in adjacent grains may vary between 0 and 1. For $m' = 1$, complete compatibility exists between the slip systems in the adjacent grains, and in this case, both the slip directions and the slip planes in each grain will be parallel. Such deformation would be expected to be easily transmitted across the grain boundary. In contrast, $m' = 0$ indicates that the slip systems are completely incompatible such that either the slip directions or slip planes are orthogonal. Such systems

J. LUSTER, Research Scientist, is with CASTOLIN, St. Sulpice, Switzerland. M.A. MORRIS, Professor, is with the Institute of Structural Metallurgy, University of Neuchâtel, Neuchâtel, Switzerland.

Manuscript submitted June 30, 1994.

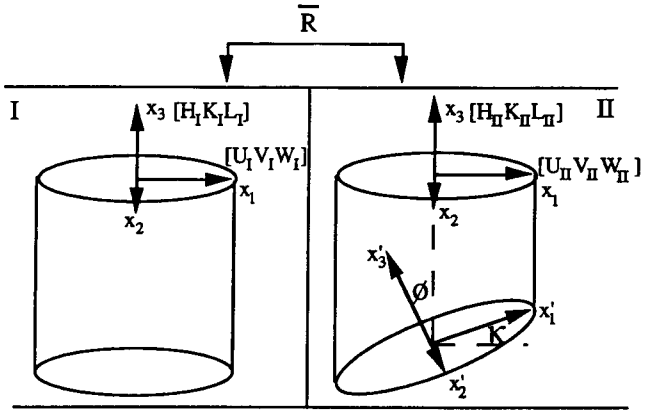

Fig. 1—Schematic diagram showing the representation of slip systems in adjacent grains from which we see the two angles, κ and ϕ, used to determine the geometric compatibility factor.

would be expected to result in unfavorable conditions at the grain boundaries. In general, m' will assume intermediate values between 0 and 1. In order to calculate this geometric parameter, it is necessary to be able to express the appropriate directions in grain I in the coordinate system of grain II or *vice versa*. This can be done easily if the orientation relationship between the two grains can be defined by an appropriate rotational matrix, $\bar{R}$.[17] Finally, the choice of the symbol m' in this text has been used to emphasize the similarity of this factor to the more commonly used Schmid factor, m. The latter represents the ratio of the resolved shear stress to the axial stress. In a similar way, the compatibility factor, m', resolves the strain due to slip in grain I onto the slip systems in the adjacent grain II.

II. EXPERIMENTAL

The material used for this study was an alloy of nominal composition Ti-47.5Al-2.5 Cr (at. pct), which was kindly supplied by Alusuisse-Lonza (Neuhausen, Switzerland). To obtain microstructures with different lamellar and equiaxed distributions of the phases, two different heat treatments were performed as follows:

(1) anneal at 1270 °C for 64 hours and cool to about 300 °C and then an anneal at 1000 °C for 5 hours, followed by a furnace cool to ambient temperature (≈5 °C/min);
(2) Anneal at 1000 °C for 168 hours, followed by a furnace cool.

For these heat treatments, the samples were encapsulated in quartz tubes that were evacuated and backfilled with argon several times prior to being sealed under argon at ≈2/3 atmospheric pressure. Cylindrical samples with a diameter of 3 mm and 6 mm in length were prepared from the as-cast and heat-treated materials and compressed to about 2 pct strain at room temperature. From these deformed samples, disks were cut perpendicularly to the compression axis and used for the analysis by TEM of the dislocations present. Thin foils were prepared by standard electropolishing techniques using a solution of 8 pct perchloric acid in 92 pct methanol at −40 °C and 15 V. A PHILIPS* CM12 electron microscope operating at 120 kV was used, and controlled tilting of the specimens was carried out using a double tilt stage. Dislocation analysis was carried out from projected images taken under different diffraction conditions obtained after tilting the specimens to different zone axes using Kikuchi maps corresponding to the $L1_0$ and DO_{19} structures. From each zone axis, different diffraction vectors were chosen to obtain invisibility under two contrast conditions. This allowed unambiguous determination of the possible Burgers vectors, as this was defined by the vectorial product of the two diffraction vectors for which invisibility occurred.

*PHILIPS is a trademark of Philips Electronic Instruments Corp., Mahwah, NJ.

A detailed determination of the orientation relationships between adjacent γ grains was carried out in the transmission electron microscope by tilting to at least three different zone axes. Due to the lower symmetry of the $L1_0$ structure in comparison with the related face-centered cubic unit cell, the choices for indexing a zone axis corresponding to an observed diffraction pattern are correspondingly reduced since [110] ≠ [101] or [011], *etc.* In order to index two or more grains related by the orientation relations described in Section I, the electron beam is oriented such that it is simultaneously parallel to a zone axis within each grain. This is generally possible when the zone axes in the adjacent grains are perpendicular to the axes of rotation defining the rotation relationship between the two grains. If a minimum of two zones is observed, for a given sense of rotation, the orientation of the axis and absence or presence of superlattice reflections can be used to define the rotation as a multiple of 60 deg rotation about the ⟨111⟩ pole.[11] This rotation was then confirmed by locating a third axis that was preferably not contained in this plane of rotation. It should also be noted that both the 60 and 300 deg or the 120 and 240 deg rotations are crystallographically equivalent rotations; thus, for any two adjacent grains, the relationship could be equally described by 60 or 300 deg (or 60 deg clockwise rotation and 60 deg anticlockwise). However, if a collection of more than two grains is examined, then there will be a difference between adjacent grains rotated by 60 or 300 deg, and it is necessary to appreciate this difference in order to correctly determine the unique orientation relationships. Proper indexing of all related grains was necessary in order to be able to determine the deformation mechanisms in a spatially consistent manner as required by the geometric compatibility factor calculations described in Section I.

III. RESULTS

A. *Initial Microstructures*

The microstructure of the initial as-cast alloy consists of large, fully lamellar grains that are composed of alternating lamellae of the γ-TiAl (imaged dark) and the α_2-Ti_3Al (light) phases, as shown in Figure 2(a). The heat treatment at 1270 °C for 64 hours retains the grain shape and size from the original as-cast structure; however, the distribution of lamellae is seen to have been

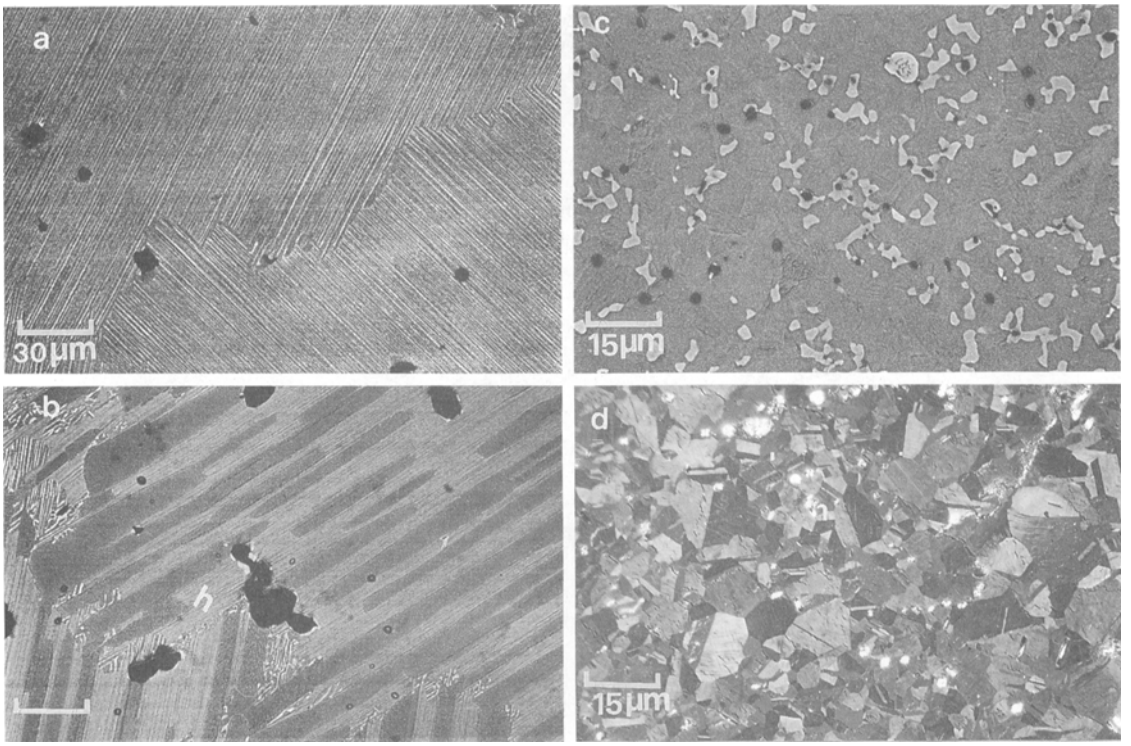

Fig. 2—Microstructures observed using backscattered electrons in the SEM from the different heat treatments: (*a*) as-cast starting material, (*b*) transformed lamellar structure after anneal at 1260 °C, (*c*) globular α_2 particles distributed within the γ matrix observed after the heat treatment at 1000 °C, and (*d*) the same microstructure as (c) but obtained using polarized light in the optical microscope to produce a crystallographic contrast in order to observe the equiaxed γ domains constituting the matrix phase.

altered by the heat treatment, as shown in Figure 2(b). This transformed lamellar structure consists of approximately 50 pct coarse γ lamellar regions and 50 pct fine lamellar regions. The average thickness, t, of the coarse γ regions is about 8 μm; the fine lamellar regions consist of alternating γ (t = 105 nm) and α_2 (t = 55 nm) lamellae. It should be noted that the expected orientation relationship was confirmed to exist between the two phases. Consequently, the orientation relationship between adjacent γ lamellae may also be described as a multiple of 60 deg rotation about a $\langle 111 \rangle$ pole. It is also seen in Figure 2(b) that limited discontinuous coarsening has also occurred at the grain boundary regions. In contrast, an equiaxed microstructure was created during the 1000 °C/168 h heat treatment, as shown in Figures 2(c) and (d). This microstructure consists of a matrix of 90 pct γ phase constituted by equiaxed domains (average size 5 to 10 μm) with 10 pct small elongated α_2 particles. Although the latter are seen in Figure 2(c), obtained by atomic number contrast in the scanning electron microscope (SEM), only the equiaxed γ domains are observed in Figure 2(d) when polarized light is used in the optical microscope so as to obtain crystallographic contrast. The orientation relationships found between adjacent γ domains are the same as noted in the lamellar structures. In contrast, no specific epitaxial relationship was found between the γ and α_2 particles. Also, some black particles are observed in all three alloy conditions that have been identified as aluminum oxides. Since these particles were present in the as-cast alloy and their size and distribution are unchanged after heat treatment, they are attributed to contamination in the casting and are not due to further oxygen pickup during the heat treatments.

B. *Deformation Behavior*

A typical example obtained after deformation of the equiaxed microstructure is shown in Figure 3. Here we see an arrangement of four γ grains (indicated as A, B, E, and F) of average size 10 μm and coarse α_2 particles, which are frequently located at the boundaries between the γ grains. The orientation relationships between adjacent grains have been determined as described in Section I from the corresponding diffraction patterns shown in Figure 4 and obtained from tilting experiments. The orientation of the patterns and the presence of superlattice reflections in zones 1 and 2 are used to identify the relationships, and the $\langle 100 \rangle$-type zone is then used as a confirmation of the relationships that have been summarized at the bottom of Figure 4. Individual deformation structures have not been identified within the α_2 particles, indicating that deformation of the alloy is accomplished mainly by deformation in the γ phase. The active deformation mechanisms are seen to vary from grain to grain. Contrast analysis of areas B and F showed that these grains deformed primarily by the glide of $1/2\langle 110]$ ordinary dislocations, while grains A and E deform by deformation twinning. Detailed contrast analysis with the twin fault invisible (*i.e.*, $g \cdot R_F = 0$, 1, or 2) was used to unambiguously confirm that only $1/6\langle 112]\{111\}$-type twinning was present as predicted.[18] A summary of deformation systems identified

Fig. 3—Typical example of a deformed equiaxed microstructure from which the rotation relationships and the active dislocations in adjacent grains have been analyzed.

in each grain is given in the schematic diagram shown in Figure 5. Also given in the diagram is the Schmid factor, m, for each of the active deformation systems. In a general manner, it should be noted that the active deformation systems correspond to those possible with the largest resolved far-field shear stress. However, exceptions to this statement occur regarding the activation of superdislocations. In each of the grains, at least one type of superdislocation had a Schmid factor greater than 0.35, yet these were not observed. This clearly indicates that deformation twinning and ordinary dislocation systems are the preferred deformation mechanisms under the current loading conditions of our alloy.

Another important and general characteristic of the equiaxed microstructure is the common occurrence of secondary deformation systems locally at grain boundaries or in the vicinity of α_2 particles. Obviously, the activation of these systems is not directly related to the Schmid factor but rather to deformation compatibility requirements. Depending upon grain orientation, ⟨101] and 1/2⟨112] superdislocations are also sometimes identified to be active throughout a grain. The role of superdislocations in the deformation process will be discussed in more detail in Section 1.

A representative example of the deformation characteristics of the transformed lamellar structure is shown in Figure 6. Four coarse γ lamellae are observed that are surrounded by zones of fine lamellae. Two types of interfacial boundaries exist between these four domains. The interfaces between lamellae A/B and E/F are flat and regular, characterized by a {111} plane. The rotation between these lamellae is most often of the 180 deg, true-twin type. The second type of boundary is that between the lamellae A/E and B/F, which separates a single lamella into two differently ordered regions. Although these interfaces are irregular in nature and cannot be described by a low-index habit plane, the rotation between these ordered domains within a single lamella can only be described as a 90 deg rotation about a cube axis (or, equivalently, 120 deg rotation about a ⟨111⟩). It is readily seen that, similarly to the equiaxed structure, the deformation systems vary from domain to domain. A summary of the deformation systems identified in each grain, the corresponding Schmid factors, and the orientation relationships between the lamellae are shown in Figure 7, which is a schematic representation of Figure 6.

1. *Influence of loading orientation*

In order to understand the variation in the active slip systems between the differently oriented grains, we have summarized the different deformation mechanisms analyzed in each grain with specific loading directions. This is shown in Figures 8(a) and (b) for the equiaxed and coarse (>1 μm) lamellar structures, respectively. The numbers seen in the projection for each orientation shown represent different slip systems present within the grains analyzed with that orientation. The numbers represent the active systems as follows: (1) twinning, (2) 1/2⟨110], (3) ⟨101], (4) 1/2⟨112], and (5) faulted dipoles. It should be noted that two or more mechanisms were always identified in each grain; therefore, at least two numbers are seen for each orientation. We confirm that deformation twinning and glide of ordinary dislocations are the dominant deformation modes since ordinary dislocations (denoted as 2) are identified in virtually every

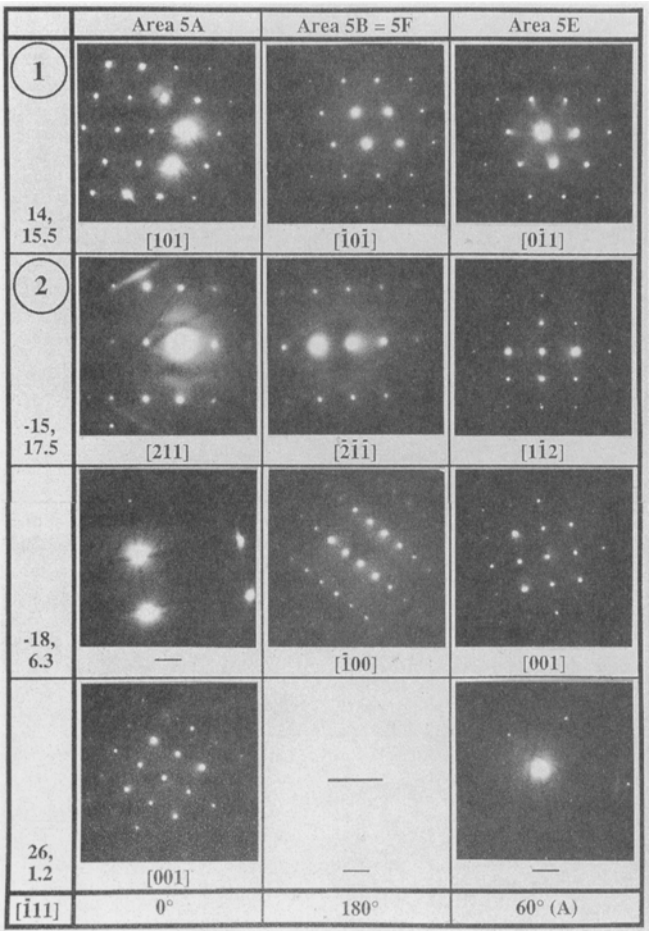

Fig. 4—Diffraction patterns corresponding to the grains A, B, E, and F from Fig. 3 obtained after tilting to the values of the angles shown on the left such that specific orientations were reached. From such patterns, the specific rotations around the axis [$\bar{1}$11] shown at the bottom have been measured.

grain in both microstructures, while twinning (denoted as 1) is identified in the majority of grains. Moreover, it should be noted that the influence of loading orientation is similar in each microstructure. Namely, deformation twinning is the primary mechanism for loading orientations around the [001] direction; ordinary dislocations are active for all orientations; and superdislocations are active for loading orientations more nearly parallel to the (001) plane. This influence of loading orientation is readily understood in terms of Schmid factor calculations. Ordinary dislocations are commonly observed for $m > 0.25$, twinning for $m > 0.25$, and superdislocations for $m > 0.35$. While these values cannot be used to determine precise values for the critical resolved shear stresses due to the polycrystalline limitations, they do indicate, in a general way, the relative preferences for the various deformation mechanisms. Hence, it is concluded that activation of ⟨101] or 1/2⟨112] superdislocations will only be possible in grains where deformation twinning is not possible due to geometric constraints. These geometric restrictions are due to the fact that twinning is only favorable in compression for loading orientations in which passage of the appropriate partial dislocations results in a compressive shape change of the material according to the polarity conditions.[19] Therefore, only for loading orientations where twinning is "forbidden" according to the polarity conditions will activation of ⟨101] or 1/2⟨112] superdislocations be possible when the appropriate Schmid factor is achieved.

It must be noted that 1/2⟨112] superdislocations are also identified in grains where the Schmid factor is below the approximate value given previously. In these cases, it can be assumed that these dislocations were either present in the heat-treated condition or that they are created due to the local stresses produced by strain incompatibility. The former is unlikely to be the case since the density of these dislocations is much greater than that observed in the as-heat treated materials, and they are

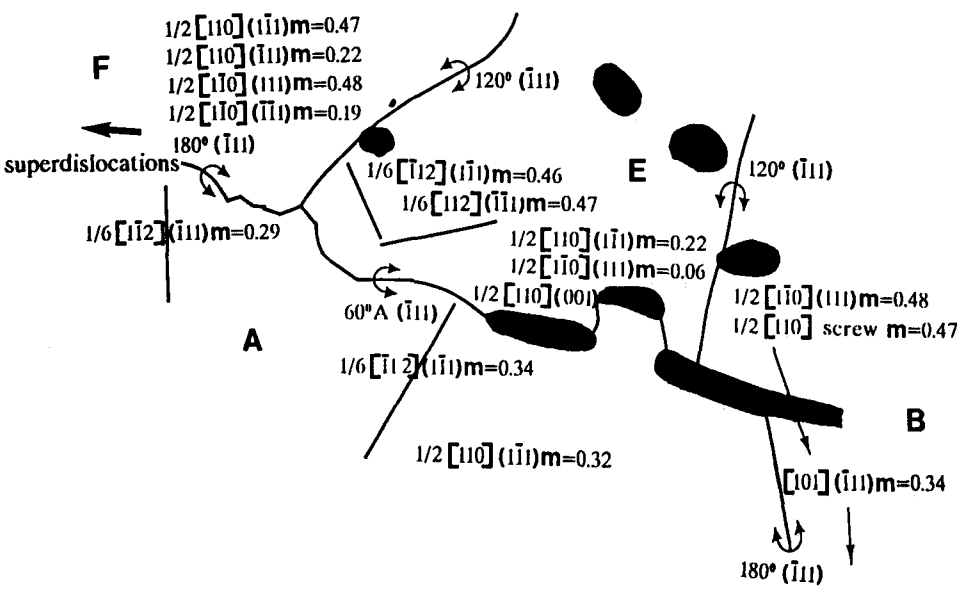

Fig. 5—Schematic diagram from Fig. 3 indicating all the active slip (or twinning) systems analyzed from each grain. Note that all the Schmid factors, m, calculated from the active systems are also shown.

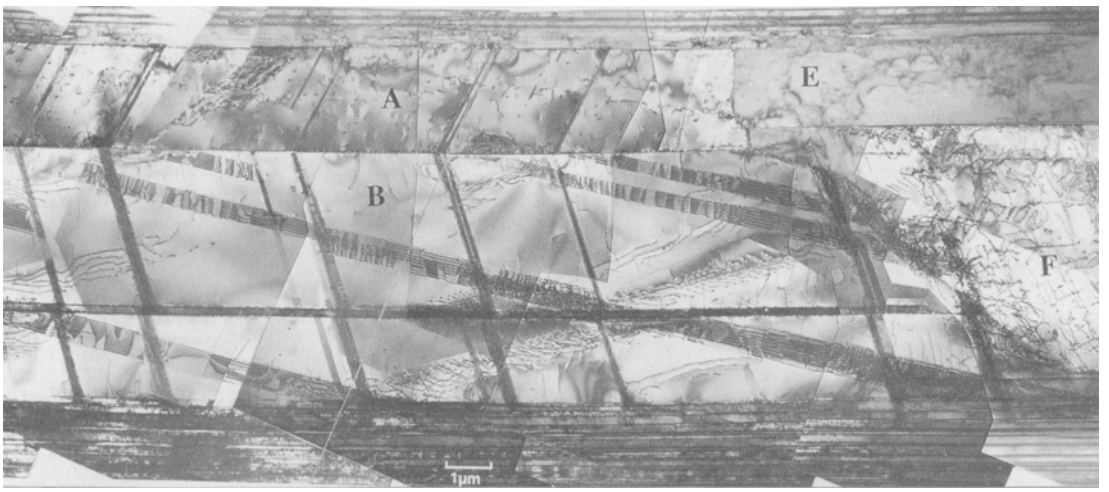

Fig. 6—Typical example from a transformed lamellar structure after 2 pct deformation from which the specific rotations and active dislocations have been analyzed in all the grains.

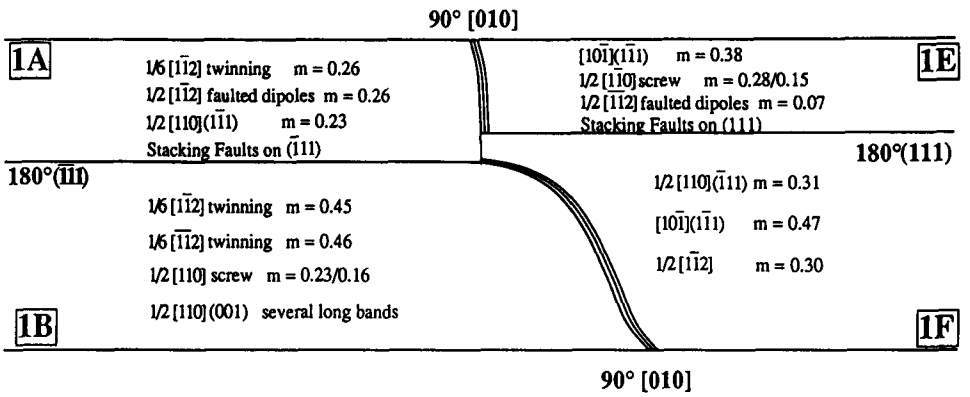

Fig. 7—Schematic diagram from Fig. 6 indicating all the active slip (or twinning) systems analyzed from each grain. Note that all the Schmid factors, m, calculated from the active systems are also shown.

systematically observed only for specific grain orientations.

Finally, faulted dipoles are frequently observed to be associated with the 1/2⟨112] superdislocations. Although these have been described in detail elsewhere,[11] it is interesting to note in Figure 8 that the formation of stacking faults and faulted dipoles (denoted as 5) is only identified for loading directions nearly parallel to a ⟨111⟩. Therefore, there are some grain orientations (*i.e.*, away from a ⟨111⟩ loading direction) where superdislocations are active, yet show little tendency to form faulted dipoles. In contrast, loading directions near ⟨111⟩ (10 to 12 deg) are usually characterized by a high density of stacking faults that are either isolated or associated with the 1/2⟨112] superdislocations. This strongly suggests that the orientation of the applied stress may play an important role in the formation of faulted dipoles.

2. *Influence of microstructure*

Although localized deformation modes are frequently observed in the equiaxed structure, they are rarely seen in the lamellar structures. This seems to indicate that the stress distribution in the equiaxed structure can be relaxed by producing deformation in adjacent γ grains, while in the lamellar structure, the stress concentrations do not appear to be readily relieved by localized plastic deformation. These differences might explain the variable ductility of these two types of microstructures commonly reported in the literature.[20]

Furthermore, it can be seen that twinning is more common in the equiaxed microstructure than in the coarse lamellae by comparison of Figures 8(a) and (b). While deformation twinning was observed in 90 pct of the equiaxed domains, it was only identified in 50 pct of the coarse lamellar grains. These observations lead to the conclusion that the stress distribution in the equiaxed microstructure is more favorable to the initiation of twinning. Since twinning has been shown to constitute an important deformation mode in these alloys at room temperature,[9] it appears evident that this different behavior should lead to greater ductility in the alloy constituted by the equiaxed domains.

Finally, we have confirmed that the lamellar thickness influences the number of deformation systems activated within the γ lamellae. In general, it has been found that all lamellae thicker than 1 μm deform by two or more deformation mechanisms, while the lamellae below this approximate limit deform primarily by only one deformation mode. Therefore, it is apparent that reducing the lamellar thickness has an effect in reducing the number of deformation systems active in the γ lamellae.

3. *Influence of orientation relationships*

The unique orientation relationships between adjacent γ grains that have been defined in Section 1 may now be exploited in order to understand the influence of the geometric compatibility of slip systems in adjacent grains on the deformation process. For this, we will describe some examples in which the compatibility factor, m', of the slip systems in adjacent grains has been calculated. The schematic diagram of Figure 9 indicates the active slip systems analyzed from the equiaxed grains F, A, and E in Figure 3. We have calculated the geometric compatibility factor corresponding to these systems from adjacent grains in an effort to understand the local activation of superdislocations observed only at the boundary between grains F and A. The geometric compatibility factors, m', between the twinning systems observed in grains E and A and all the possible slip systems that might be active in grain F are shown in Table I. Also shown in Table I are the Schmid factors corresponding to each slip system. Examination of Table I reveals that there is a good compatibility ($m' = 0.87$) between the deformation systems that have been observed in the grains E and F, and therefore, coherency is maintained at the interface with no need for additional activation of other slip systems. In contrast, part (c) of Table I shows that the compatibility of the $(1\bar{1}1)$ twinning system in grain

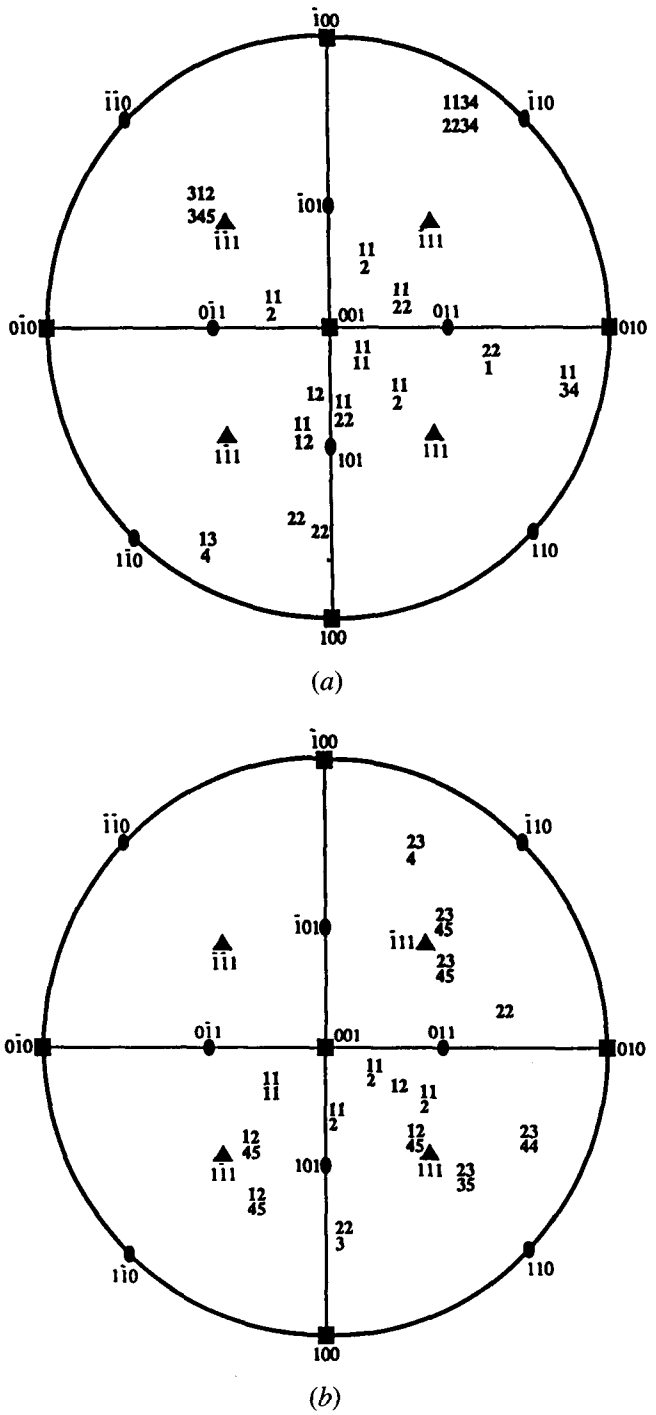

Fig. 8—Influence of the loading orientation on the active deformation mechanisms analyzed from (*a*) the equiaxed structure and (*b*) the transformed lamellar structure. The numbers seen in the projection for each orientation shown represent different slip systems present within the grains analyzed with that orientation. The numbers represent the active systems as follows: (1) twinning, (2) 1/2 ⟨110], (3) ⟨101], (4) 1/2 ⟨112], and (5) faulted dipoles. Note that two or more numbers represent the corresponding several slip systems observed.

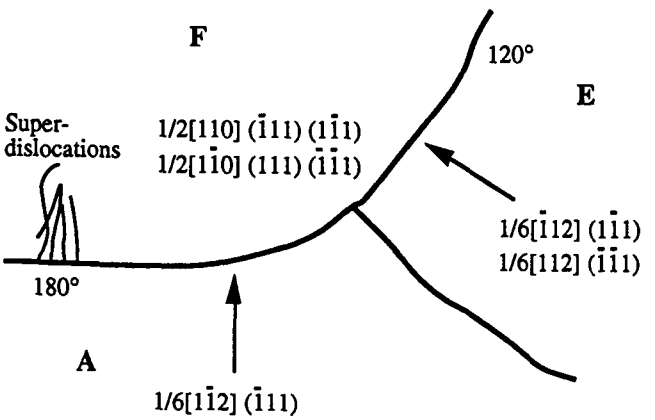

Fig. 9—Schematic diagram of the active deformation mechanisms from the equiaxed grains A, E, and F from Fig. 3.

Table I. Geometric Compatibility of Possible Slip Systems in Grain F

Possible Slip in F	m	m'	Observations
(a) With 1/6[112](1̄1̄1) twinning in grain E for a 120 deg rotation about [1̄11]			
1/2[110](1̄11)	0.47	0.87	active in F
[10̄1](1̄11)	0.32	0.87	—
[1̄12](1̄11)	0.11	0.50	—
[101](1̄11)	0.35	0.10	—
(b) With 1/6[1̄12](1̄11) twinning in grain E for a 120 deg rotation about [1̄11]			
1/2[11̄0](111)	0.49	0.87	active in F
[10̄1](111)	0.28	0.87	—
[1̄1̄2](111)	0.02	0.50	—
[101](1̄11)	0.35	0.10	—
(c) With 1/6[11̄2](1̄11) twinning in grain A for a 180 deg rotation about [1̄11]			
[11̄2](1̄11)	0.27	1.00	activated ??
[101](1̄11)	0.35	0.87	—
1/2[11̄0](111)	0.49	0.19	active in F
1/2[11̄0](1̄1̄1)	0.19	0.19	active in F
1/2[110](1̄11)	0.47	0.0	active in F
1/2[110](1̄11)	0.22	0.0	active in F

A and the ordinary dislocation systems in grain F is low ($m' = 0.19$ or 0.0). Thus, in order for coherency to be maintained at the grain boundary, additional deformation modes must be activated in either grain A or F. In this way, activation of a superdislocation system in grain F appears to be necessary in order to fulfill the required shape changes at the A/F boundary. Although exact determination of the Burgers vector of these dislocations has not been made, it is interesting to speculate that these are $1/2[1\bar{1}2]$ superdislocations since this system would exhibit complete compatibility with the twinning in grain A. Regardless of the Burgers vector of these dislocations, calculation of the compatibility between the active deformation systems in grains A and F can be used to predict the need for additional slip systems.

An example of the geometric compatibility between the deformation systems in the lamellar structure for a 120 deg rotation is given in Figure 10, which shows two thin, adjacent lamellae, labeled A and B, embedded within a large colony of γ and α_2 lamellae. In each lamella, a single deformation mechanism is active. Trace analysis was used to determine the twin system in lamella B as $1/6[\bar{1}12]$ $(1\bar{1}1)$. The Schmid factor for this twinning system is $m = 0.50$. In lamella A, a low density of individual dislocations is observed, and contrast experiments were used to confirm these to be [101] superdislocations. Subsequently, the geometric compatibility factors for possible deformation systems in lamella A with $(1\bar{1}1)$ twinning in B have been calculated as shown in Table II. Table II indicates that both the Schmid and the geometric compatibility factors are important in determining which slip systems are active in the fine lamellae. Although four to five slip systems would be possible in lamellae A solely on the basis of the Schmid factor, the actual deformation mode corresponds with the system that also maximizes the geometric compatibility between the adjacent lamellae.

An example of the compatibility of deformation systems in adjacent γ lamellae that are related by a 180 deg rotation is shown in Figure 11. Both lamellae contain only ordinary dislocations with the Burgers vector $1/2[1\bar{1}0]$. Since practically none of the $1/2[1\bar{1}0]$ dislocations are observed to be straight segments parallel to the $(\bar{1}\bar{1}1)$ lamellar interface, the slip plane of these dislocations cannot be the $(\bar{1}\bar{1}1)$ plane. Thus, the deformation system in each lamella is characterized as $1/2[1\bar{1}0]$ (111). The geometric compatibility calculations for these two systems are given in Table III. It is again observed that several possible slip systems in lamella C could be expected solely on the basis of the Schmid factor. However, the active system tends again to be that which also yields the maximum geometric compatibility.

4. *Deformation in the α_2 phase*

Although the deformation is mainly concentrated in the γ phase, a few examples of dislocations within the α_2 lamellae were also observed. One example of this is the lamellar colony shown in Figure 12. In Figure 12(a), two coarse, similarly oriented γ lamellae are seen to be

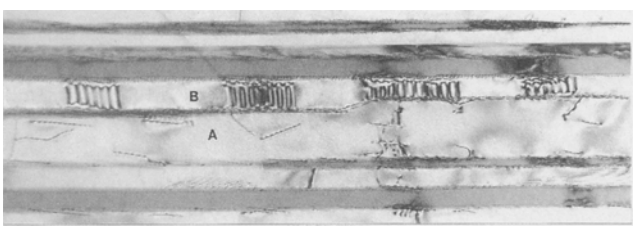

Fig. 10—Example of deformed microstructures from fine adjacent lamellae related by a 120 deg rotation.

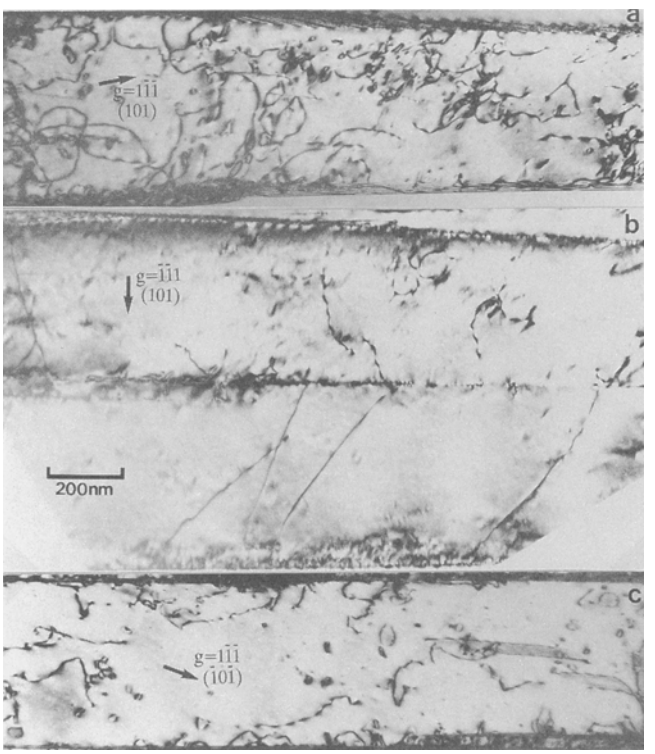

Fig. 11—Example of deformed microstructures from fine adjacent lamellae that exhibit a true-twin, 180 deg rotation relationship.

Table II. Schmid Factor and Geometric Compatibility Factor, m', for the Deformation Systems Lamella A for $1/6[\bar{1}12](1\bar{1}1)$ Twinning in the Adjacent Lamellae B

Possible Slip in A	m	m'	Observations
$[101](\bar{1}11)$	0.45	0.87	identified in B
$1/2[110](\bar{1}11)$	0.40	0.87	—
$[\bar{1}01](1\bar{1}1)$	0.45	0.10	—
$1/2[\bar{1}10](\bar{1}\bar{1}1)$	0.40	0.10	—
$1/2[110](1\bar{1}1)$	0.34	0.28	—

Table III. Geometric Compatibility for Possible Slip Systems in Lamella C for $1/2[1\bar{1}0](111)$ Dislocations in Lamella B

Possible Slip in C	m	m'	Observations
$1/2[1\bar{1}0](111)$	0.28	0.78	active in C
$1/2[1\bar{1}0](\bar{1}\bar{1}1)$	0.32	0.33	—
$[1\bar{1}2](\bar{1}11)$	0.35	0	—
$[\bar{1}\bar{1}2](111)$	0.34	0	—
$[\bar{1}12](1\bar{1}1)$	0.35	0.32	—
$[0\bar{1}1](111)$	0.42	0.39	—

separated by a coarse α_2 lamella (indicated by A). Also, within both of the γ lamellae, fine α_2 lamella are seen. In the coarse lamella, A, two different types of dislocation structures were observed. A low density of dislocations was observed throughout the thickness of the lamella, and these were distributed rather homogeneously along the length of the lamella (invisible in Figures 12(a) and (b)). Contrast experiments and trace analysis were used to determine that the Burgers vector of these dislocations is parallel to $[11\bar{2}0]$ and that they are on the $(1\bar{1}00)$ plane. The Schmid factor for this slip system is $m = 0.48$. It is interesting to note that these dislocations appear to be present either individually or in pairs (1), and that dissociations may also be possible (2).

A second type of dislocation is limited to the interface regions immediately adjacent to the γ grain as indicated by the arrows (Figure 12(b)). The contrast experiments used to identify these dislocations are shown in Figure 13. It is noted that these dislocations are visible for the $0002g$ (Figure 12) and thus must be either $\langle a \rangle$ + $\langle c \rangle$- or $\langle c \rangle$-type dislocations. However, since the dislocations are invisible for both $02\bar{2}0g$ and $2\bar{2}20g$, the Burgers vector must be parallel to [0001]. By comparison of the projected length of the dislocation under different beam directions, it can be determined that the probable slip plane is near $(1\bar{1}00)$. It must again be emphasized that these were only found as loops or short segments immediately adjacent to the interface and were often associated with a twin in the γ lamella. The Schmid factor for this system is only $m = 0.05$, and thus, it is unlikely that these can be attributed directly to the effect of the applied load. To understand the activation of this localized dislocation system, the geometric compatibility factors were calculated in relation to the deformation mechanisms in the surrounding γ phase—the twinning system $1/6[\bar{1}\bar{1}2]$ (111). Using the specific orientation relationship between the γ and α_2 phases as $[\bar{2}110]_{\alpha_2}//$

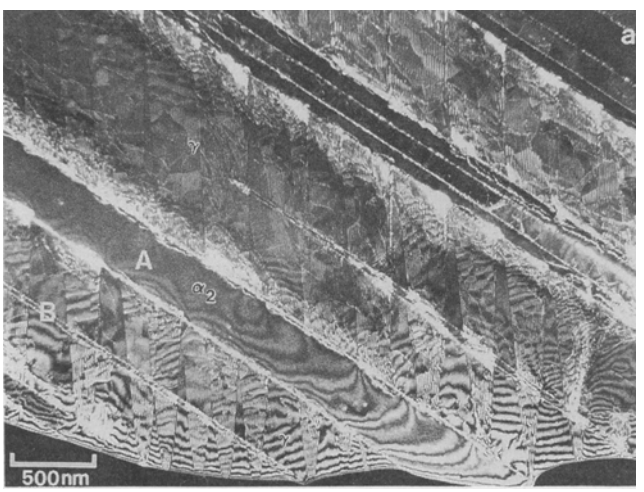

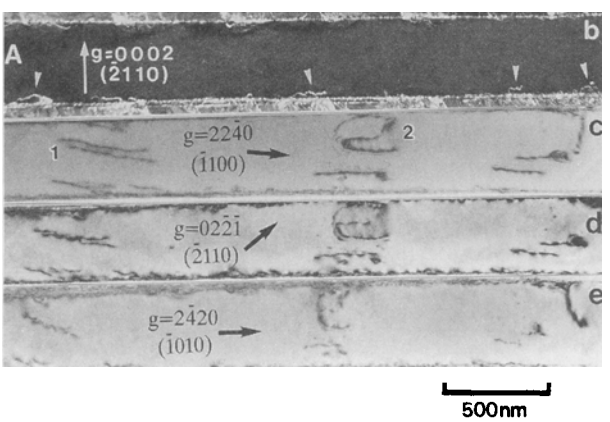

Fig. 12—(*a*) General deformed microstructure from a typical lamellar zone. (*b*) through (*e*) Different diffraction conditions used to analyze dislocation segments within the α_2 phase. Note the short segments marked by the arrows at the γ/α_2 interface in (b).

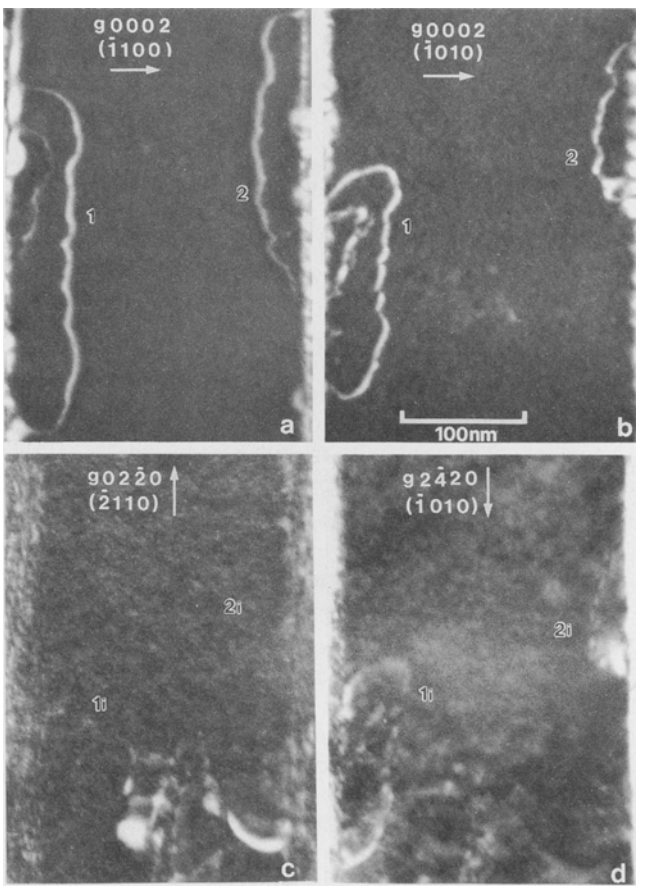

Fig. 13—(*a*) through (*d*) Detailed weak beam images under different diffraction conditions used to identify the bowed dislocation segments confined to the interfacial region in the α_2 lamella A of Fig. 12(b).

Table IV. Geometric Compatibility Factors for Possible Slip Systems in the α_2 Lamella for Twinning on the (111) Plane in the Adjacent γ Lamellae

Slip Direction	Slip Plane	m'	Comments
[0001]	$(1\bar{1}00)$	0.88	maximum compatibility
$[\bar{1}2\bar{1}6]$	$(1\bar{2}11)$	0.84	—
$[\bar{2}116]$	$(2\bar{1}\bar{1}1)$	0.84	—
[0001]	$(2\bar{1}\bar{1}0)$	0.77	—
$[2\bar{1}\bar{1}0]$	$(01\bar{1}0)$	0.14	highest for a prismatic slip system
$[11\bar{2}0]$	$(\bar{1}100)$	0.00	observed in interior of the lamella

$[011]_\gamma$, the compatibility factors have been calculated and are shown in Table IV.

The results shown in Table IV can be shown to explain the appearance of the [0001] dislocations in the interfacial region. The compatibility factor shows that the $[11\bar{2}0]$ dislocations, while active within the lamellae due to the applied shear stress, provide little compensation for the shape changes in the surrounding γ lamellae due to (111) twinning. However, it is the [0001] $(1\bar{1}00)$ slip system that provides the maximum compatibility with the twinning in the γ lamellae. Therefore, it is suggested that these [0001] dislocations in the α_2 lamella are created due to the shape changes imposed by the (111) twinning and, as such, serve to accommodate the stresses created at the γ/α_2 interface. The general observation that these dislocations are usually associated with the twins in γ supports this conclusion. However, the short distances that these dislocations propagate from the interface indicate that they have only a low mobility. Due to this limited mobility, they can only partially accomplish the imposed shape changes. Since the prismatic $\langle 11\bar{2}0\rangle$ dislocations appear to have higher mobility (since they are found at the interior of the grains), they would appear to be a more favorable system to activate in order to accommodate the stress concentrations. However, the geometric compatibilities for these $\langle 11\bar{2}0\rangle$ slip systems are all rather low, with the maximum compatibility factor for a prismatic slip system being only $m = 0.14$. Thus, while the prismatic family of dislocations may be rather mobile, they do not provide the required shape changes necessary to maintain compatibility at the interface with the adjacent γ lamellae.

IV. DISCUSSION

Through determination of the precise spatial relationship between grains and the subsequent application of the geometric compatibility factor, it has been shown that the orientation relationship does indeed influence the deformation process. The significance of the orientation relationship is that it geometrically defines the relative alignment of slip systems in adjacent grains.

Experimentally, application of the geometric compatibility factor in both the equiaxed and lamellar microstructures has shown the following.

(1) The geometric compatibility factor could be applied in the equiaxed microstructure to predict the activation of the slip systems at the grain boundary or at a pileup.
(2) The geometric compatibility factor plays an important role in the activation of the deformation modes in the fine lamellar structures.
(3) In general, the orientation relationship defined by a 120 deg-type rotation provides the maximum compatibility between slip systems in adjacent grains.

In order to fully understand the influence of these orientation relationships, it is necessary to examine the geometry of intersecting slip systems at grain boundaries, as shown schematically in Figure 14. Here we see a {111} slip plane in the initial grain I intersecting the boundary plane of an adjacent grain designated II. For both the 60 deg pseudotwin and 180 deg true-twin relationships, the angles formed at this boundary between the slip plane

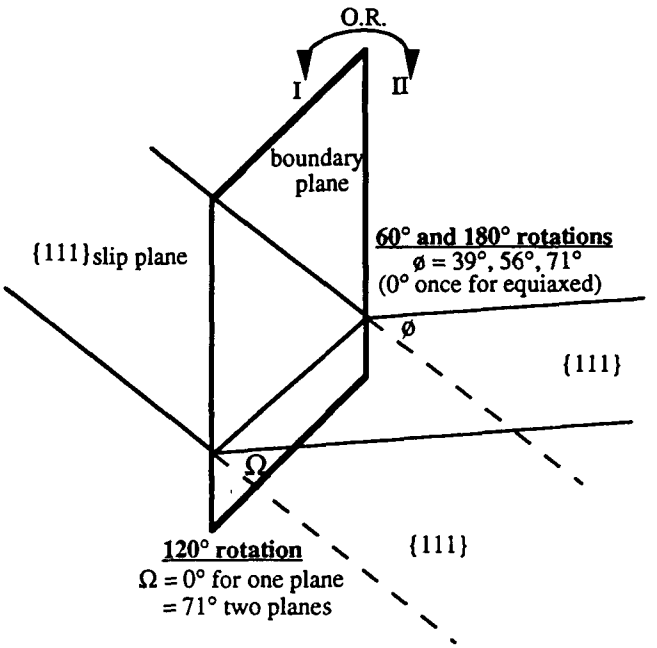

Fig. 14—Influence of the rotation between two adjacent grains, I and II, on the geometry of the intersection of possible slip planes in each grain.

in grain I and the possible {111} slip planes in grain II are ϕ = 39, 56, or 71 deg. Additionally, if the deformation in grain I occurs on the {111} plane used as the defined plane of rotation, then obviously this plane will be parallel to the same plane in grain II (in which case the other three {111} planes all intersect this plane of rotation at an angle of 71 deg). Although it has been observed that deformation parallel to the interfacial plane is rare for the lamellar structures, this has been identified in the equiaxed microstructure. Therefore, ϕ = 0 deg has also been indicated in the diagram for the equiaxed structure only.

Alternatively, a completely different geometric situation can be identified for a 120 deg rotation. For a {111} slip plane defined in grain I, one possible slip system in grain II will form an angle of 0 deg with this original plane, while the other two {111} planes will form a 71 deg angle. Thus, for any {111} slip plane in grain I, there exists a {111} glide plane in grain II that corresponds exactly to the original slip plane. Thus, deformation on {111} planes in grain I could be transmitted directly to the corresponding {111} plane in grain II (*i.e.*, Ω = 0 deg) with relatively little resistance. In this case, the transfer mechanisms would then depend upon the Burgers vector of the slip systems involved.

The importance of the direction of the Burgers vectors can be understood in a general way by applying the specific rotations on a $\langle 111\rangle$ projection or using the standard rotational matrix transformation. There will, in general, be no correspondence between $\langle 101\rangle$ or $\langle 112\rangle$ slip directions in grains I and II when they are related by 60 and 180 deg rotations. The exception to this is again when the directions lie in the {111} plane used to define the orientation relationship. In this case, the directions in each grain will exactly correspond. This behavior directly contrasts the geometric situation for grains related

by 120 deg rotation, where each ⟨110⟩ slip direction in grain I will be parallel to a ⟨110⟩ direction in grain II. Although the ⟨112⟩ family of directions would also be parallel in each grain, the $L1_0$ ordering imposes restrictions such that slip is only possible in the ⟨112] direction. Hence, ⟨112] in grain I will be parallel to a ⟨211] direction in the related grain, but this ⟨211] is not a possible slip direction. Thus, although there is an exact correspondence between the ⟨110⟩ slip directions in the two grains, this is not the case for the ⟨112] directions.

With the possible geometric arrangements of slip systems completely defined, the maximum geometric compatibility factor for each slip system as a function of orientation relationship can be calculated. Listed in Table V are all of the possible slip systems considered for an initial grain I and the maximum compatibility factor that would result for the slip system in the adjacent grain II and the type of slip system corresponding to this maximum value.

In correspondence with the experimental observations, Table V shows that the slip systems in adjacent grains related by a 120 deg rotation can always result in better compatibility than either the 60 or 180 deg rotation. The exceptions to this are, naturally, the slip systems contained within the {111} plane of rotation, in which case the geometric compatibility factors are either 0.87 or 1.00 for all rotations. Therefore, it is possible to hypothesize that the transfer of slip between adjacent grains will be the easiest for a 120 deg rotation due to the good geometric alignment of slip systems. In contrast, transfer of slip across grain boundaries between grains related by 60 and 180 deg rotations would be expected to be more difficult due to the lower geometric compatibility. Since the equiaxed structure is composed of a random arrangement of orientation relationships (and, therefore, contains many favorable 120 deg rotations) while the lamellar structure is dominated by the 180 deg rotation, it could be expected that the equiaxed structures would generally be more ductile than the lamellar ones.

Table V. Influence of Orientation Relationship on the Maximum Compatibility Factor for Rotations about [$\bar{1}\bar{1}1$]*

Slip System I		Maximum Compatibility Factor in II		
b	(*hkl*)	60 deg	120 deg	180 deg
110	$\bar{1}11$	0.65 O	1.00 S	0.65 S
110	$1\bar{1}1$	0.65 S	1.00 S	0.65 S
$1\bar{1}0$	111	0.78 S	1.00 S	0.78 O
$1\bar{1}0$	$\bar{1}\bar{1}1$	1.00 S	1.00 S	1.00 O
112	$\bar{1}\bar{1}1$	0.87 S	0.87 O	1.00 112
$\bar{1}12$	$1\bar{1}1$	0.67 O	0.87 O	0.67 S
$1\bar{1}2$	$\bar{1}11$	0.73 112	0.87 O	0.67 S
$\bar{1}\bar{1}2$	111	0.54 S	0.87 O	0.60 112
101	$\bar{1}11$	0.78 S	1.00 O	0.78 S
101	$\bar{1}\bar{1}1$	1.00 S	1.00 O	1.00 S
$10\bar{1}$	111	0.65 O	1.00 O	0.65 S
$10\bar{1}$	$1\bar{1}1$	0.65 S	1.00 O	0.65 O
011	$1\bar{1}1$	0.78 O	1.00 S	0.78 S
011	$\bar{1}\bar{1}1$	1.00 O	1.00 S	1.00 S
$01\bar{1}$	111	0.65 S	1.00 S	0.65 S
$01\bar{1}$	$\bar{1}11$	0.65 S	1.00 S	0.65 O

*Type of slip system that gives this compatibility: S ⟨101] superdislocation system, O an ordinary 1/2⟨110] dislocation system, and 112 slip or twinning in a ⟨112] direction.

The geometric compatibility factor can also be used to understand the transmission of slip across the α_2 lamellae. In Table IV, only the case of (111) twinning in an adjacent γ lamella was examined. Since there are three possible twinning systems in the γ lamellae, the geometric compatibilities have been calculated for the three twinning systems and are summarized in Table VI. Here it is readily seen that the $(1\bar{1}1)$ and $(\bar{1}11)$ twinning systems result in geometrically equivalent relationships with the possible slip systems in α_2 and that they exhibit a different geometry from that of (111) twinning. According to critical resolved shear-stress calculations and TEM studies of the deformation mechanisms, it is known that the $\langle 2\bar{1}\bar{1}0\rangle$ $\{01\bar{1}0\}$ prismatic slip systems are the most favorable in the α_2 phase. Therefore, it is clear that the two geometric situations will vary in their ability to accommodate twinning in the adjacent γ lamellae. For (111) twinning, the maximum compatibility factor for a favorable prismatic slip system is only $m' = 0.14$. Therefore, these favorable dislocations will not be able to accommodate the twinning in the adjacent γ lamellae, and as a result, unfavorable [0001] or ⟨1216⟩ pyramidal dislocations will be necessary. In contrast, for the other two twinning systems, there exists a prismatic $\langle 11\bar{2}0\rangle$ system that gives a geometric compatibility of $m' = 0.82$ for the adjacent twinning. Due to this higher compatibility, glide of the prismatic dislocations will effectively be able to accommodate the adjacent twinning deformation and, therefore, reduce stress concentrations at the interface. Based on this analysis, fracture at the α_2/γ interface is predicted to occur preferentially when (111) twinning is activated in the γ phase due to the low compatibility of this particular twin system with a favorable prismatic slip system in the α_2 phase.

Many investigations have shown that the mechanical properties of TiAl alloys may be varied through thermomechanical processing.[21,22] Moreover, it has frequently been reported that the equiaxed microstructures are more ductile than lamellar ones. This cannot be attributed to the influence of loading orientation since our study has shown that the latter is similar in each microstructure; *i.e.*, the specific slip systems were activated for the same values of Schmid factors (≥0.25) in each type of microstructure (Section 3–A–1). On the other hand, it has been confirmed that the equiaxed structure exhibits greater activation of twinning and of local slip systems in response to stress concentrations. Therefore, it appears that this local driving force for deformation, together with the fact

Table VI. Maximum Geometric Compatibility Factors for the Possible Slip Systems in an α_2 Lamella for the Given Twinning System in the Adjacent γ Lamellae Using $[\bar{2}110]_{\alpha_2}//[011]_\gamma$ and $(0001)_{\alpha_2}//(\bar{1}\bar{1}1)_\gamma$

(111) Twinning		$(1\bar{1}1)$ Twinning		$(\bar{1}11)$ Twinning	
$[0001](1\bar{1}00)$	0.88	$[\bar{2}110](01\bar{1}1)$	0.84	$[\bar{1}2\bar{1}0](\bar{1}011)$	0.84
$[\bar{1}2\bar{1}6](1\bar{2}11)$	0.84	$[\bar{2}110](01\bar{1}0)$	0.82	$[\bar{1}2\bar{1}0](\bar{1}010)$	0.82
$[\bar{2}116](2\bar{1}\bar{1}1)$	0.84	$[1126](11\bar{2}1)$	0.63	$[11\bar{2}6](\bar{1}\bar{1}21)$	0.63
$[0001](2\bar{1}\bar{1}0)$	0.77	$[2\bar{1}\bar{1}0](0\bar{1}11)$	0.50	$[1\bar{2}10](10\bar{1}1)$	0.50
$[2\bar{1}\bar{1}0](01\bar{1}0)$	0.14				

that the equiaxed structure will on average contain more 120 deg-type boundaries which will provide more favorable opportunities for slip transmission, will account for a better ductility of the equiaxed structures. Similarly, the possibility of slip on the plane used to define the rotation between grains also provides favorable modes of slip transmission and is only possible in the equiaxed structure. These observations also suggest that ductility of lamellar alloys can be optimized by controlling the γ lamellae thickness to 1 μm or more while minimizing the thickness of the α_2 lamellae. If the dominant γ/α_2 interface of the lamellar alloys could be replaced with favorable 120 deg γ/γ interfaces, the optimum ductility of the lamellar structure could be expected to be achieved.

V. CONCLUSIONS

The effect that varying distributions of γ and α_2 phases have on the specific rotation relationships between γ/γ and γ/α_2 grains in a Ti-47.5Al-2.5Cr alloy has been studied. These specific rotation relationships have been used to understand their effect on the compatibility of deformation across adjacent γ grains.

It has been shown that orientation relationships described by a 120 deg rotation will provide the best compatibility between slip systems in adjacent grains. In the lamellar structure, the majority of orientation relationships between γ lamellae are the 180 deg true-twin type, while the distribution of orientation relationships in the equiaxed structure is random. Thus, more of the favorable 120 deg type will be present in the equiaxed structure, which will be expected to exhibit better ductility due to an easier slip transfer across the γ grains.

Also, in the case of the lamellar structures, the α_2 lamellae limit the deformability of the γ lamellae by restricting the propagation of slip. In this case, the lamellar thickness plays an important role in the deformation process, with more slip systems being activated in the case of γ lamellae thicker than 1 μm but only single deformation mechanisms being present in the case of thinner lamellae.

REFERENCES

1. Y.-W. Kim and D.M. Dimiduk: *J Met.*, 1991, vol. 8, p. 40.
2. V.K. Vasudevan, M.A. Stucke, S.A. Court, and H.L. Fraser: *Phil. Mag. Lett.*, 1989, vol. 59, p. 299.
3. H. Inui, M.H. Oh, A. Nakamura, and M. Yamaguchi: *Phil. Mag. A*, 1992, vol. 66, p. 557.
4. S.C. Huang and E.L. Hall: *Metall. Trans. A*, 1991, vol. 22, pp. 427-39.
5. M.A. Morris: *Phil. Mag. A*, 1993, vol. 68, p. 237.
6. M.J. Blackburn: in *The Science, Technology and Applications of Titanium*, R. Jaffee and N.E. Promisel, eds., Pergamon Press, New York, NY, 1970, p. 633.
7. H. Inui, M.H. Oh, A. Nakamura, and M. Yamaguchi: *Phil. Mag. A*, 1992, vol. 66, p. 539.
8. T. Kawabata, M. Tadano, and O. Izumi: *Scripta Metall.*, 1988, vol. 22, p. 1725.
9. M.A. Morris: *Phil. Mag. A*, 1993b, vol. 68, p. 257.
10. Y. Umakoshi and T. Nakano: *Acta Metall.*, 1993, vol. 41, p. 1155.
11. J.W. Luster: Ph.D. Thesis, University of Neuchâtel, Neuchâtel, Switzerland, 1994.
12. J.D. Livingston and B. Chamlers: *Acta Metall.*, 1957, vol. 5, p. 322.
13. S. Muira, K. Hamashima, and K.T. Aust: *Acta Metall.*, 1980, vol. 28, p. 1591.
14. C. Rey and A. Zaoui: *Acta Metall.*, 1982, vol. 30, p. 523.
15. H. Kawazoe, T. Takasugi, and O. Izumi: *Acta Metall.*, 1989, vol. 37, p. 2883.
16. Z. Shen, R.H. Wagoner, and W.A. Clark: *Acta Metall.*, 1988, vol. 36, p. 3231.
17. W. Bolimann: *Crystal Lattices, Interfaces and Matrices*, 1982, Springer-Verlag, Berlin, p. 44.
18. D.W. Pashley, J.L. Robertson, and M.J. Stowell: *Phil. Mag. A*, 1969, vol. 19, p. 83.
19. E. Schmid and W. Boas: *Kristallplastizität*, Julius Springer, Berlin, 1935.
20. Y.-W. Kim: *J. Met.*, 1980, vol. 7, p. 24.
21. Y.-W. Kim: *Acta Metall.*, 1992, vol. 40, p. 1121.
22. W.O. Soboyejo, D.S. Schwartz, and S.M.L. Sastry: *Metall. Trans. A*, 1992, vol. 23, pp. 2039-59.